*sustainability*

MDPI

*Article*

# In Vitro Cytocompatibility Assessment of Novel 3D Chitin/Glucan- and Cellulose-Based Decellularized Scaffolds for Skin Tissue Engineering

**Kannan Badri Narayanan [1,2,*], Rakesh Bhaskar [1,2], Hyunjin Kim [1] and Sung Soo Han [1,2,*]**

[1] School of Chemical Engineering, Yeungnam University, 280 Daehak-Ro, Gyeongsan 38541, Gyeongbuk, Republic of Korea; indiaxenobiotic@gmail.com (R.B.); hj0156@yu.ac.kr (H.K.)
[2] Research Institute of Cell Culture, Yeungnam University, 280 Daehak-Ro, Gyeongsan 38541, Gyeongbuk, Republic of Korea
* Correspondence: okbadri@gmail.com or okbadri@yu.ac.kr (K.B.N.); sshan@yu.ac.kr (S.S.H.)

**Abstract:** Background: Naturally derived sustainable biomaterials with high flexibility, mechanical properties, biocompatibility, and the ability to manipulate surface chemistry, providing a natural cellular environment, can be used for tissue engineering applications. However, only a few researchers have demonstrated the exploitation of natural architectures for constructing three-dimensional scaffolds. The chemical decellularization technique for fabricating natural scaffolds and their cytocompatibility assessment for tissue engineering applications need to be thoroughly explored and evaluated. Methods: Decellularization of natural scaffolds has been performed via a chemical method using anionic detergent sodium dodecyl sulfate (SDS) which was used for the in vitro culturing of murine embryonic NIH/3T3 fibroblasts. Techniques such as field-emission scanning electron microscopy (FE-SEM), compressive testing and swelling ratio, and biodegradation were performed to characterize the properties of fabricated decellularized natural scaffolds. Nucleic acid quantification, DAPI, and H&E staining were performed to confirm the removal of nuclear components. In vitro cytocompatibility and live/dead staining assays were performed to evaluate cultured fibroblasts' metabolic activity and qualitative visualization. Results: 3D chitin/glucan- and cellulose-based scaffolds from edible mushroom (stem) (DMS) and unripe jujube fruit tissue (DUJF) were fabricated using the chemical decellularization technique. FE-SEM shows anisotropic microchannels of highly microporous structures for DMS and isotropic and uniformly arranged microporous structures with shallow cell cavities for DUJF. Both scaffolds exhibited good mechanical properties for skin tissue engineering and DUJF showed a higher compressive strength (200 kPa) than DMS (88.3 kPa). It was shown that the DUJF scaffold had a greater swelling capacity than the DMS scaffold under physiological conditions. At 28 days of incubation, DUJF and DMS displayed approximately 14.97 and 15.06% biodegradation, respectively. In addition, DUJF had greater compressive strength than DMS. Compared to DMS scaffolds, which had a compressive stress of 0.088 MPa at a 74.2% strain, the DUJF scaffolds had a greater compressive strength of 0.203 MPa at a 73.6% strain. The removal of nuclear DNA in the decellularized scaffolds was confirmed via nucleic acid quantification, DAPI, and H&E staining. Furthermore, both of these scaffolds showed good adherence, proliferation, and migration of fibroblasts. DMS showed better biocompatibility and high viability of cells than DUJF. Conclusions: This sustainable scaffold fabrication strategy is an alternative to conventional synthetic approaches for the in vitro 3D culture of mammalian cells for various tissue engineering and cultured meat applications.

**Keywords:** biomaterial; chemical decellularization; scaffold; fungus; fibroblast; skin tissue engineering



**Citation:** Narayanan, K.B.; Bhaskar, R.; Kim, H.; Han, S.S. In Vitro Cytocompatibility Assessment of Novel 3D Chitin/Glucan- and Cellulose-Based Decellularized Scaffolds for Skin Tissue Engineering. *Sustainability* **2023**, *15*, 15618. https://doi.org/10.3390/su152115618

Academic Editor: Marko Vinceković

Received: 21 September 2023
Revised: 18 October 2023
Accepted: 2 November 2023
Published: 4 November 2023



## 1. Introduction

Skin is the largest organ in the human body and is a barrier in protecting the body from harsh outside conditions. It also helps regulate body temperature and preserves the body's

hydration. In addition, it also helps in self-healing via immunological processes [1]. The skin has three layers: the outermost thin epidermis, the innermost hypodermis layer, and the dermis layer in the middle. The dermis layer provides mechanical strength to the skin and it consists of fibroblasts and the extracellular matrix (ECM) such as glycosaminoglycans, fibrin, fibronectin, proteoglycans, elastin, and collagens [2]. Damage to the skin in traumatic injury causes an imbalance in physiological functions and leads to death. Skin damage can come from burns, chronic wounds and infections, acute trauma, and surgical interventions. The majority of minor skin wounds can heal on their own. Still, certain deep partial- or full-thickness skin wounds that are >4 cm in depth take longer to heal naturally and require surgery, as well as skin substitutes for skin repair and regeneration [3]. Split skin grafts (SSG) of healthy skin comprising the epidermis and a part of the dermis layers are generally used to cover the areas of damaged skin of non-healing wounds. SSG grafting facilitates the transfer of self-renewing keratinocyte stem cells to the wound area to initiate and be involved in the rapid healing processes and skin regeneration [4]. However, SSG for full-thickness wounds causes hypertrophic scars/keloid formation, limits the utilization of SSG, and requires ideal alternative techniques for wound healing.

The recent advancements in tissue-engineered skin substitutes have made them a therapeutic option for skin regeneration and wound healing [5]. These tissue-engineered skin substitutes must be biocompatible, biodegradable, nontoxic, and provide the required mechanical strength for proper functioning. It should also mimic a three-dimensional (3D) cellular environment for cell adherence, proliferation, and migration, providing a natural cellular milieu for skin tissue engineering applications [6]. Developing tissue-engineered biomaterials with a desired architecture supporting in vitro cell growth and function has gained attention recently. Generally, scaffolds with high porosity and interconnected pores allow for the movement of cultured cells, the diffusion of nutrients and signaling molecules, the removal of waste, and mechanical support mimicking the anatomical structure [7]. It should also elicit minimal immunogenicity, antigenicity, and inflammatory responses with enhanced angiogenesis. Natural polymers, such as alginate, chitosan, chitin, bacterial cellulose, cellulose, or collagen, and synthetic polymers, such as poly(vinyl) alcohol, poly(ethylene glycol), polycaprolactone, or polylactic acid, are used to fabricate biocompatible skin tissue-engineered (STE) scaffolds with well-defined porosity and excellent mechanical properties [8]. Furthermore, different composite biomaterials were prepared with a combination of synthetic and natural polymers to improve the mechanical and other desired characteristics of scaffolds for skin tissue engineering.

Over the past few decades, several advances have been made in developing cost-effective and sustainable biomaterials as skin substitutes for skin regeneration and wound healing. Recently, decellularization via chemical, physical, and enzymatic techniques was used to remove cellular components from animal tissues, and the retained intact structural framework of ECM, which provides the mechanical properties of native tissue, was used as an intriguing strategy in the fabrication of novel scaffolds [9]. Chemical decellularization using ionic surfactant sodium dodecyl sulfate (SDS) can efficiently remove cellular and genetic materials. Decellularization of several tissues and organs using SDS, including porcine cornea, myocardium, heart value, lungs, kidney, and human vein and lungs, were previously reported [10]. Nevertheless, using decellularized animal-derived scaffolds is expensive, with ethical controversy [11]. Therefore, to meet the challenges, the chemical decellularization of sustainable materials, viz., mushroom- and fruit-derived tissues, with ideal characteristics for the 3D fabrication of tissue-engineered constructs, can be used for various tissue engineering applications. Decellularized fungus and fruit tissues resemble the native tissues of animals with similar microporosity and topography and an ideal pore size of 50–200 μm in diameter [12]. Mushrooms and fruits of angiosperms are highly diverse; therefore, these biomaterials as scaffolds can provide different topography, porosity, and pore size for culturing other mammalian cells for biomedical applications [13]. In our study, we chemically decellularized mushroom (*Agaricus bisporus*) and unripe jujube fruit

(*Ziziphus jujuba*) and characterized and evaluated the cytocompatibility of these scaffolds for culturing embryonic mouse fibroblasts for skin tissue engineering applications.

## 2. Experimental

### *2.1. Materials*

Edible basidiomycete mushroom (*Agaricus bisporus*) and unripe Jujube fruit (*Ziziphus jujuba*) were purchased from the agricultural market in Gyeongsan, Republic of Korea. Sodium dodecyl sulfate (SDS) and calcium chloride ($CaCl_2$) were purchased from Duksan Pure Chemicals Co., Ltd. (Ansan-si, Gyeonggi-do, Republic of Korea). The embryonic murine fibroblast cell line NIH/3T3 (CRL-1658) was obtained from the American Type Culture Collection (Manassas, VA, USA). Fetal bovine serum (FBS), penicillin/streptomycin, and 1X trypsin-EDTA were purchased from Gibco$^{TM}$ (Thermo Fisher Scientific, Inc., Waltham, MA, USA).

### *2.2. Decellularization of Mushroom- and Fruit-Based Scaffolds*

The decellularization of mushroom (*Agaricus bisporus*) and unripe jujube fruit (*Ziziphus jujuba*) was performed via a chemical method as described previously by Hickey et al. [14] with modifications. Briefly, mushroom (gills and stem) and unripe jujube fruit were transversely cut in circular dimensions with a ~1–2 mm thickness using a mandolin slicer. Later, the samples were put into a 250 mL conical beaker containing 100 mL of SDS (0.5% *w*/*v*) and stirred at 150 rpm at room temperature for 24 h. After SDS treatment, the samples were washed several times with deionized water, transferred into a 100 mM $CaCl_2$ solution, and stirred at room temperature for 24 h to remove any residual surfactant, followed by washing in deionized water three times. The decellularized scaffolds of the mushroom stem, mushroom gills, and unripe jujube fruit were named DMS, DMG, and DUJF, respectively. These scaffolds were then sterilized in 70% ethanol and freeze-dried for 48 h after pre-incubating at −80 °C for 6 h for further experiments (Figure 1).

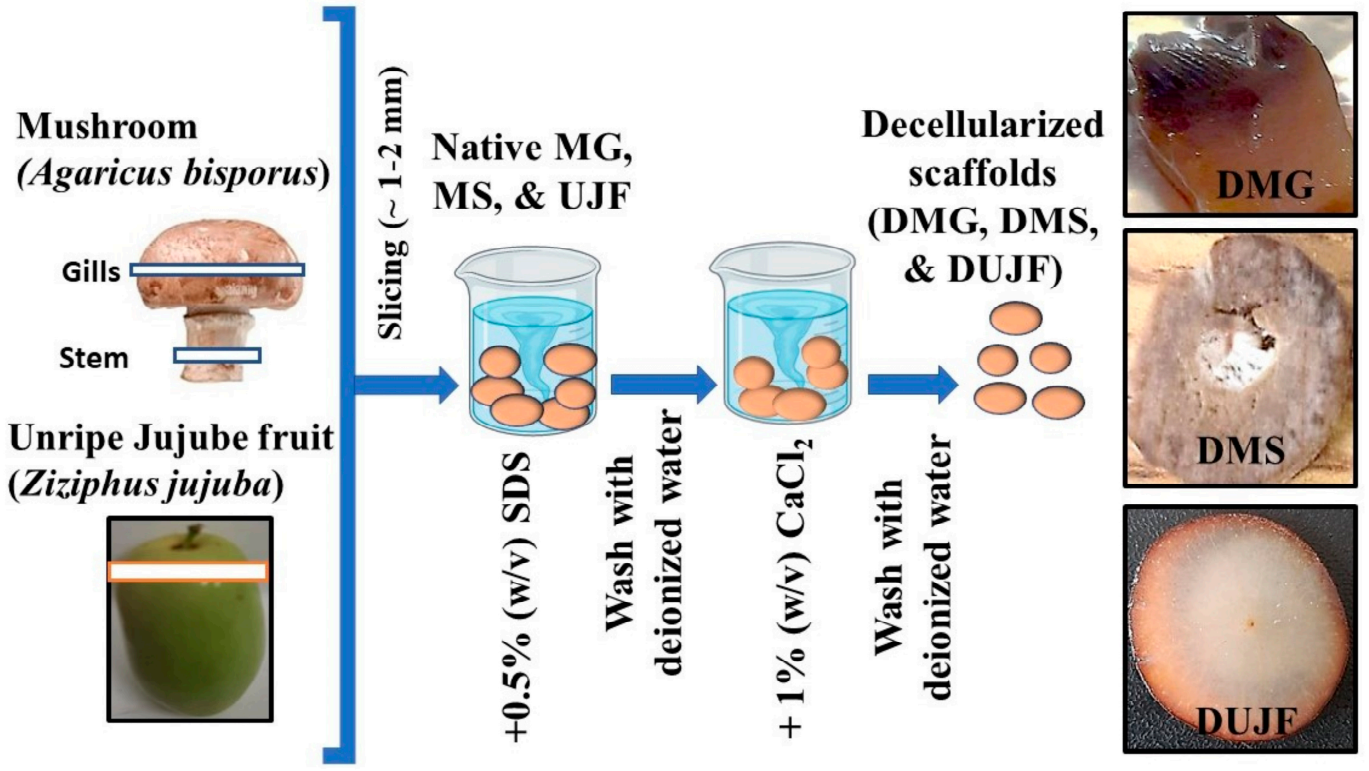


**Figure 1.** Schematic diagram representing the fabrication of decellularized scaffolds of the mushroom gills (DMG), mushroom stem (DMS), and unripe jujube fruit (DUJF).

### 2.3. Characterization of Native and Decellularized Scaffolds

After sputter coating with platinum on an aluminum stub, the morphology of the decellularized scaffolds was observed using a Hitachi (Model: S-400) field-emission scanning electron microscope (FE-SEM) at 10 kV. Attenuated total reflectance-Fourier transform Infrared spectroscopy (ATR-FTIR) was performed on Spectrum 100 (PerkinElmer, Waltham, MA, USA) to analyze the chemical components of native and decellularized scaffolds.

The compressive strength of circular scaffolds (DMS; 8 mm × 2.6 mm, and DUJF; 7.3 mm × 2 mm) (diameter × height) was evaluated using a tabletop universal testing machine (force tester) (Model: MCT-2150; A&D Company Ltd., Tokyo, Japan) under compression mode with a load cell of 500 N.

The percentages of the porosity, swelling ratio, and degradation of scaffolds were calculated as described earlier [4,14]. The swelling ratio (%) was determined with the formula:

$$[(W_t - W_0)/W_0] \times 100 \quad (1)$$

where $W_0$ is the initial weight of the freeze-dried scaffold, and $W_t$ is the weight of the scaffold at a specific time interval (phosphate-buffered saline (PBS) at 37 °C and 50 rpm). The sample weight before and after the degradation period and the average percentage of residual weights for DUJF and DMS were calculated. The decellularized scaffolds (DMS and DUJF) were weighed before and after immersion in absolute ethanol using the liquid displacement method. The porosity (η) in percentage was calculated using the formula:

$$\eta = [(W2 - W1)/(\rho V1) \times 100] \quad (2)$$

where W1 and W2 are the masses of decellularized scaffolds before and after immersion, respectively. V1 is the volume of scaffolds and ρ is the density of the ethanol.

Native and decellularized scaffolds were used for deoxynucleic acid (DNA) quantification. DNA was isolated from native- and decellularized chitin/glucan- and cellulose-based scaffolds (DMS and DUJF) using a protocol based on phenol/chloroform/isoamyl alcohol [15]. DNA quantification was performed using the Nanodrop method [16]. To ascertain the lack of genetic material in the decellularized scaffolds, DMS and DUJF were stained with DAPI staining and visualized under a fluorescent microscope [13]. Moreover, the native and decellularized scaffolds were characterized by hematoxylin and eosin (H&E) staining to assess decellularization. The thin sections of native MS, native UJF, DMS, and DUJF scaffolds were fixed with 2.5% buffered glutaraldehyde at 4 °C overnight. The scaffolds were then stained with the hematoxylin solution for 6 h, washed thoroughly with tap water, then counterstained with an eosin Y solution for 48 h and dehydrated with 95% and 100% ethanol [17,18].

### 2.4. Cell Culture

Embryonic murine fibroblasts (NIH/3T3) were cultured on a 75 $cm^2$ cell culture flask (Corning) using Dulbecco's modified Eagle's medium (DMEM, Gibco) containing 5% fetal bovine serum and 1% penicillin/streptomycin in a 5% $CO_2$ incubator at 37 °C. After 7 days of incubation, the confluent cells were trypsinized using 1 mL of 1X trypsin-EDTA and the detached cells were transferred into a 15 mL Falcon tube and centrifuged at 1000 rpm for 5 min. The pelleted fibroblasts were resuspended in a fresh DMEM-complete medium and counted with a hemocytometer.

### 2.5. Cytotoxicity Assay

The in vitro cytotoxicity of decellularized scaffolds was evaluated using an MTT assay [19]. The scaffolds (14 mm diameter × 2 mm thickness) were sterilized in 70% ethanol and washed in the DPBS and DMEM medium overnight. These scaffolds were placed in a 24-well plate and fibroblasts (~5000 cells/well) were seeded and cultured in DMEM-complete media for up to 7 days, with a change in media every 2 days. After 1, 3, 5, and 7 days of incubation, the media was removed and the wells were washed with

DPBS, and 100 µL of the MTT solution (5 mg/mL) and 100 µL of serum-free DMEM media were added to each well and incubated at 37 °C for 4 h. After incubation, 250 µL of DMSO was added to dissolve the MTT formazan crystals and the absorbance was read at 570 nm using a microplate reader. Fibroblasts cultured on tissue culture plastic (TCP) were used as the controls.

### *2.6. Live/Dead Cell Viability Assay*

LIVE/DEAD$^{TM}$ viability kit (Invitrogen, Thermo Fisher Scientific, USA) was used to qualitatively evaluate the viability of NIH/3T3 fibroblasts on scaffolds. After culturing fibroblasts on scaffolds for different periods, the media was discarded and washed with DPBS and 20 µL of the live/dead solution was added and incubated at 37 °C in the dark for 30 min and observed under an inverted fluorescent microscope (Nikon Eclipse Ti, Tokyo, Japan). To morphologically evaluate the adherence and proliferation of cells on scaffolds, these cultured scaffolds were fixed with 2.5% glutaraldehyde and dehydrated through increasing concentrations of ethanol, freeze-dried, and sputter coated with platinum before being observed in a field-emission scanning electron microscope (FE-SEM, Hitachi S-4800, Hitachi, Ltd., Chiyoda City, Tokyo, Japan).

### *2.7. Statistical Analysis*

Statistical analysis was performed using a two-way ANOVA followed by Bonferroni's post-hoc tests with significance levels at * $p < 0.05$ and ** $p < 0.01$ with GraphPad Prism 5.0 software. All data were reported as mean ± standard deviation.

## 3. Results and Discussion

### *3.1. Characterization of Decellularized Scaffolds*

Various materials of natural origin have been attempted as scaffolds for tissue engineering. Due to their diversified structural organization, surface topography, porosity, and other intriguing characteristics of the supporting matrix, these biomaterials of biological origin are potential natural sources that must be evaluated. Decellularized materials from animals, plants, and fungi are commonly assessed for their biocompatibility for state-of-the-art applications in tissue engineering and biomedicine [20]. Decellularization removes the nuclear and cytoplasmic components, which primarily trigger immune responses and leave behind the three-dimensional structural microarchitecture. These decellularized materials can be used for structural and functional applications repopulated with different cell types (epithelial, endothelial, myoblast, or neuron) for the skeletal, muscular, nervous, circulatory, or cardiovascular systems [21]. However, biological scaffold materials of plant origin are superior to those of animal origin due to their lack of immunogenicity and other adverse effects. Moreover, plant- and mushroom-based scaffolds are cost-effective and sustainable [22,23]. Esmaeili et al. [24] decellularized the Alstroemeria flower stem and modified it with chitosan to fabricate a new scaffold for soft and hard tissue engineering. Very recently, Ahmadian et al. [25] developed a novel 3D natural scaffold from decellularized tomato thorny leaves and used it as an ideal candidate for in vitro 3D hepatocellular carcinoma modeling.

Mushrooms are conspicuous large fruiting bodies with sturdy architecture and multicellular mycelium, which gives them the primary option for choosing the fabrication of scaffolds. *Agaricus bisporus* is an edible mushroom belonging to the kingdom of basidiomycetes. The gills (lamellae) and stem (stape) of *A. bisporus* were cut and decellularized to remove the cellular biomolecules such as glucose, N-acetylglucosamine, and glucosamine, along with small quantities of mannose, galactose, xylose, and amino acids [26]. The inner layer of the hyphal wall is composed of chitin microfibrils in a β-glucan matrix with proteins, whereas the outer layer contains β-glucan mucilage [27]. Furthermore, the pulp of unripe jujube fruit contains cells with a cell wall structure composed of cellulose. Decellularization removes biomacromolecules and nucleic acids from cellular components and leaves behind a highly porous framework structure. These non-cellular biocomponents

of tissues filled up in the intercellular spaces are attributed to the structural and biochemical constituents of scaffolds, which mimic the natural extracellular matrix (ECM) environment of the in vivo tissue. Chitin/glucan and cellulose are the major structural components of various living cells. Noda et al. [28] demonstrated that cellulose- and chitin/glucan-based polysaccharide nanofibers promote the adhesion, migration, and proliferation of mouse fibroblasts. Figure 2 shows FE-SEM micrographs of the surface morphology of the decellularized scaffolds, DMG, DMS, and DUJF. DMG has long stipes of hyphal structure with microspherical and elliptical spores on its surface. At the same time, DMS is a highly microporous structure with tunnel-like cell wall cavities (microchannels) in the size of 8.75 ± 6.0 µm, which can facilitate the transfer of nutrients and oxygen throughout the scaffold for the growth of mammalian cells. Natural decellularized vegetal materials as scaffolds have diverse topographies that otherwise need to be synthetically fabricated by 3D printing, electrospinning, wet spinning, or micro-groove fabrication to display specific topographies. DUJF scaffolds look isotropic, whereas DMS shows anisotropic features.

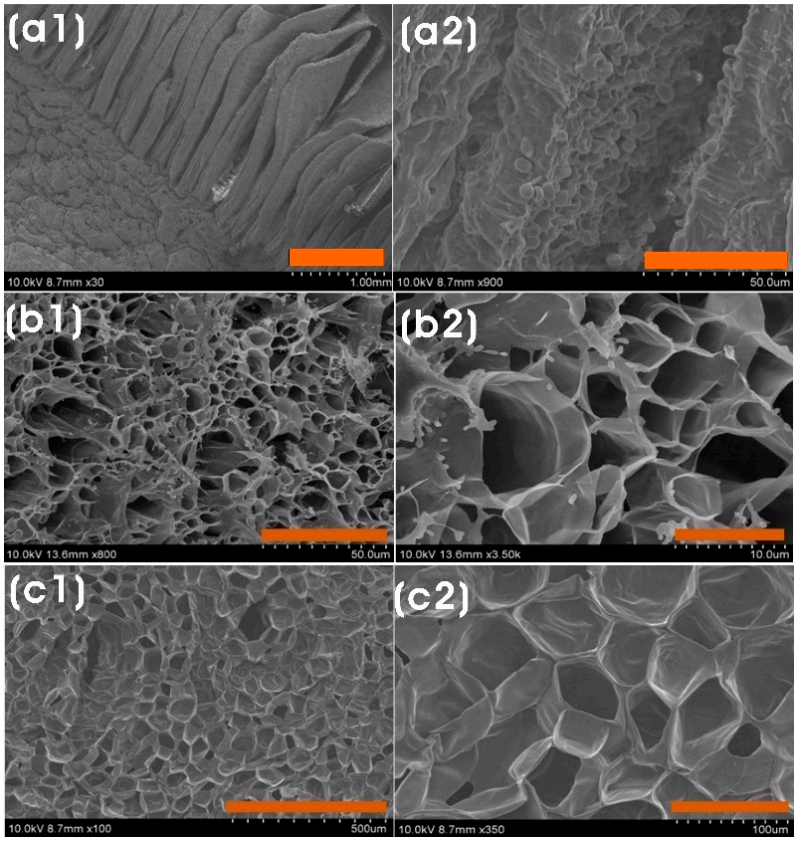


**Figure 2.** FE-SEM images of (**a1**,**a2**) DMG, (**b1**,**b2**) DMS, and (**c1**,**c2**) DUJF scaffolds.

The cellular organization and alignment of scaffolds are prerequisites for forming higher structures. The longitudinal, uniaxial alignment of myoblasts on a decellularized green onion scaffold is required to form myotubes [29]. In the case of DUJF, it is an evenly porous structure with shallow cell cavities with insufficient interconnected pores in the size range of 56.14 ± 13.9 µm. Porosity and pore size are essential factors for nutrient and oxygen delivery, allowing cells to grow inward to form a 3D tissue-like construct. DUJF scaffolds have 50.6 ± 14.6 porosity, whereas DMS has 33.78 ± 16.7. Salehi et al. [30] decellularized spinach leaf and used it as a scaffold, which showed a specific surface area, total pore volume, and mean pore diameter of 28.5 m/g, 0.0625 Cm/g, and 8.7 mm, respectively. The best characteristics of a matrix are those that stop inflammatory responses and safeguard the host tissue. The three-dimensional porosity of decellularized scaffolds facilitates the proliferation, migration, and diffusion of nutrients, signaling molecules, and

oxygen. The scaffold matrices also serve as adhesion sites for the adherence of proliferating cells [31].

In DMG and DMS, the glucan–chitin framework structure was observed and the cellulose framework structure was observed in DUJF. In both cases, no cell organelles or other identifiable structures were witnessed. DMG, with a multi-layered structure lacking pores and connectivity, is not suitable for the 3D culture of fibroblasts. SDS, an anionic detergent, was used to decellularize the mushroom- and fruit-based scaffolds and it is toxic to cells [32]. The complete removal of detergent is indispensable for the efficient adhesion, migration, proliferation, differentiation, and invasion of cells on these scaffolds. Hence, the $Ca^{2+}$ divalent cations, which can alter the critical micelle concentration of the surfactant and form insoluble micelles, were used to remove the residual SDS from the scaffolds, providing the cytocompatibility for cell adherence, proliferation, and invasion [33,34].

Figure 3 shows the FTIR of native unripe jujube fruit (UJF) and DUJF scaffolds. Figure 3a shows the commercial cellulose with 3325 $cm^{-1}$ assigned to the stretching of hydroxyl (O-H) groups. The bands at 2872 $cm^{-1}$ and 1375 $cm^{-1}$ were assigned to the stretching and deformation vibrations of the C-H group in glucose units. A low-intensity band at 894 $cm^{-1}$ was characteristic of the glycosidic linkage between glucose monomers in cellulose [35]. Moreover, the band at 1026 $cm^{-1}$ corresponds to the -C-O- group of secondary alcohols and ethers in the cellulose chain backbone. Both native UJF and DUJF show cellulosic components, of which the structural components are both UJF and DUJF scaffolds. Figure 3b shows the FTIR spectra of the native mushroom stem (MS) and DMS. The -OH stretching vibrations in phenol or $H_2O$ were at 3257 $cm^{-1}$. The band at 2922 $cm^{-1}$ was attributed to the symmetric $CH_3$ stretching and asymmetric $CH_2$ stretching, and the band at 1633 $cm^{-1}$ was due to the C=O stretching vibration of the amide I, the N-H bending of the flavonoids, and the aromatic ring deformations [36]. The band at 1402 $cm^{-1}$ was attributed to the symmetric stretching vibrations of $COO^-$ fatty acids and amino acid groups, the symmetric bending modes of methyl groups in skeletal proteins, and the symmetric stretch of methyl groups in proteins [37]. The band at 1570 $cm^{-1}$ was obtained from the N-H bending and C-N stretching vibrations of amide II proteins. These (1550 and 1402 $cm^{-1}$) bands indicate protein content in the mushroom, which decreased in decellularized DMS. The C=O stretching of the pyranose compounds in carbohydrates was shown in the 1030 $cm^{-1}$ band [38].

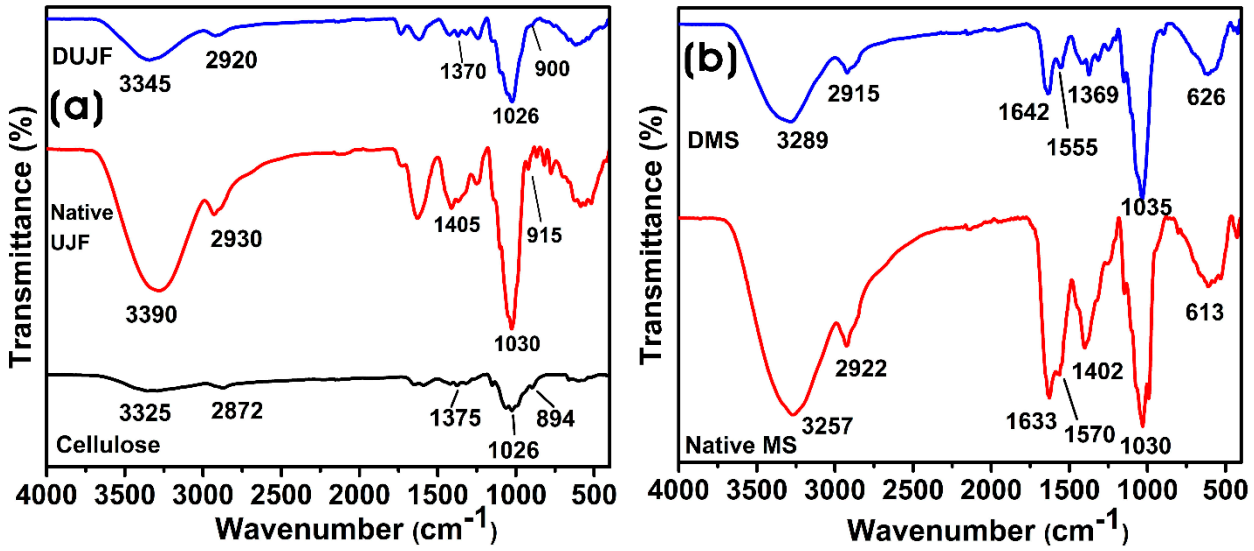


**Figure 3.** FTIR spectra of (**a**) DUJF, native UJF, and cellulose (commercial), as well as (**b**) DMS and native MS.

DNA quantification of native and decellularized scaffolds was performed (Figure 4). DMS and DUJF showed a DNA content of 0.08 ± 0.006 and 0.048 ± 0.003 ng of DNA/mg

wet weight, respectively, whereas their corresponding native materials showed 3.82 ± 0.07 and 3.7 ± 0.48 ng of DNA. Thus, the DNA content was significantly ($p < 0.01$) reduced compared to the native materials, where only 2.11 and 1.2% of the initial DNA from native material remained in the decellularized scaffolds of DUJF and DMS, respectively. It was proposed by Crapto et al. [39] that less than 50 ng of double-stranded deoxynucleic acid (dsDNA) per milligram dry weight of the extracellular matrix (ECM) of native material is allowed in decellularized biomaterials for in vivo applications. The light microscopic images of DUJF and DMS are shown in Supplementary Figure S1. Light microscopic images of DUJF and DMS show the ECM framework of the cell structure. Supplementary Figure S2 shows the DAPI staining of the decellularized and native scaffolds. After the decellularization process, the nuclear materials from DMS and DUJF were comparatively less than the native materials. The outer cell wall structure of cellulose and the chitin/glucan were preserved in decellularized scaffolds. Supplementary Figure S3 shows the H&E staining of native and decellularized scaffolds. There were very few nuclear components; only red-stained ECM was observed after the decellularization process compared to the native components. Moreover, the cell wall structure in the decellularized scaffolds was intact for tissue engineering.

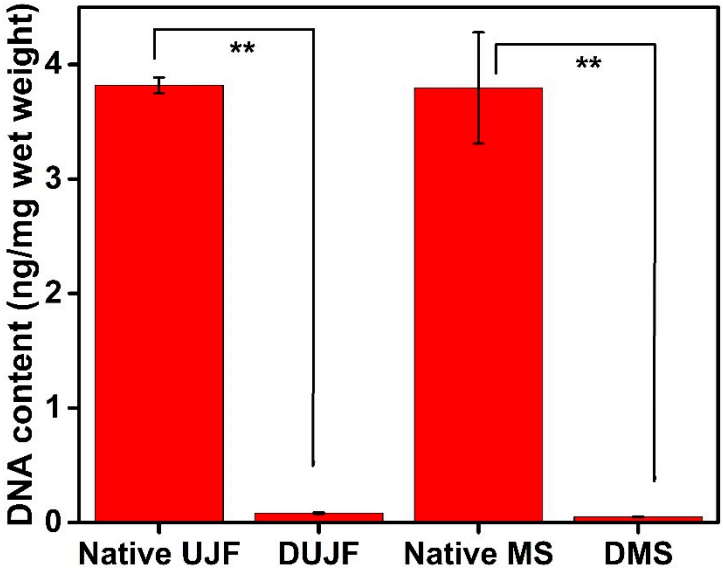


**Figure 4.** Quantification of DNA content of native and decellularized scaffolds.

DMS and DUJF scaffolds comprise chitin–glucan and cellulosic frameworks, respectively, with densely packed polymeric chains. It provides interaction between water and the hydroxyl (-OH) and carboxyl (-COOH) groups of the polymeric chains of the structural framework. Figure 5a shows the swelling ratio of DMS and DUJF scaffolds. It was observed that the swelling capacity of DUJF was higher than the DMS scaffold in PBS (pH 7.4). Indeed, after 5 min, the scaffolds sharply reached a percentage of the swelling ratio of 1379.4 ± 241.5% and 821.9 ± 52.5% for DUJF and DMS, respectively. Thereafter, there was only a slight increase which reached equilibrium values with a mass swelling ratio of 1694.4 ± 223.8 and 1063.18 ± 163.25% at 240 min. This swellable property is highly desirable for biomedical applications of scaffolds under physiological conditions [40,41].

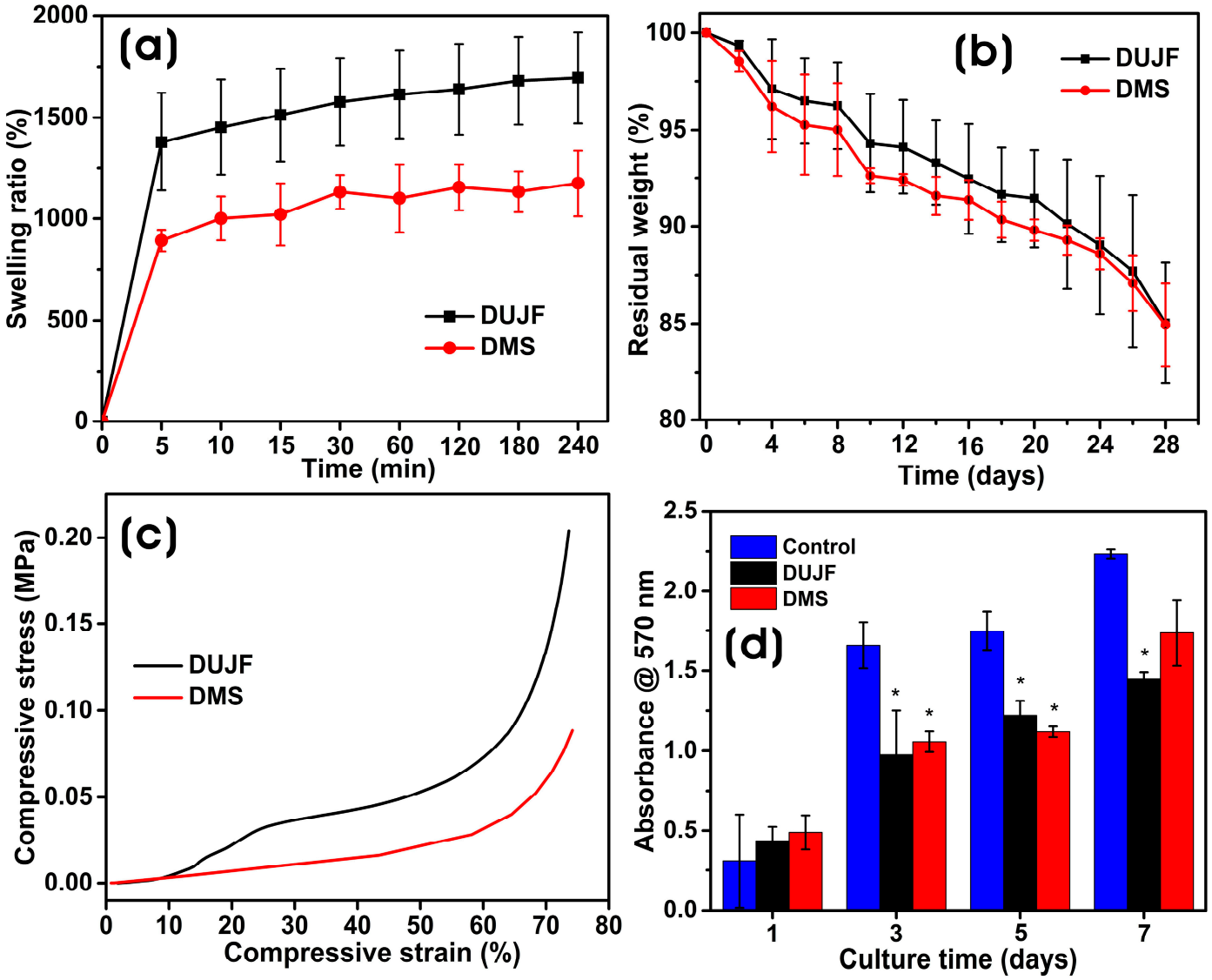


**Figure 5.** (**a**) Swelling ratios, (**b**) residual weight percentage during 28 days of degradation, and (**c**) compressive stress–strain curves of DUJF and DMS scaffolds in PBS (pH 7.4) at 37 °C and 50 rpm. (**d**) Quantitative evaluation of the cellular activity of NIH/3T3 fibroblasts in DUJF and DMS scaffolds up to 7 days.

The biodegradation property of scaffolds is closely connected to the structural architecture and cell behavior needed to support tissue regeneration. The degradation of DUJF and DMS was measured in PBS (pH 7.4) at 37 °C and 50 rpm and the results are illustrated in Figure 5b. Cellulose-based DUJF scaffolds exhibit a lower biodegradation rate than chitin/glucan-based DMS scaffolds under physiological conditions. DUJF and DMS showed approximately 14.97 ± 0.5 and 15.06 ± 0.38% degradation in 28 days of incubation under physiological conditions. DUJF showed a sustainable weight loss on incubation, whereas DMS showed a drastic change in weight loss after 4 days. Mushroom-based scaffolds contain chitin/glucan and elastic and hydrophobic polymeric rubber-like protein resilin, which resists its easy degradation like cellulose-based frameworks [42]. At the same time, cellulose-based polymeric materials contain long-chain glucose polymers that are firmly bound with other plant components, such as hemicellulose and lignin, providing high resistance to hydrolysis.

Decellularized scaffolds must possess a certain level of mechanical strength to enable cell development and the production of cell layers so that they can withstand the weight

of the cultured cells in their swollen state. Figure 5c shows the compression performance of the fully swollen DMS and DUJF scaffolds. The compressive strength of DUJF was higher than that of DMS. The DUJF scaffolds achieved a higher compressive strength of 0.203 MPa at a 73.6% strain compared to DMS scaffolds with a compressive strength of 0.088 MPa at a 74.2% strain. It is clear from the results that DUJF scaffolds with a cellulose architecture are mechanically stronger than DMS scaffolds, primarily with a chitin/glucan structure. Negrini et al. [43] reported that the decellularized apple-derived cellulosic scaffolds exhibited a decrease in stiffness and maximum compressive stress at 30%. The equilibrium compressive aggregate modulus of articular cartilage ranges between 0.1 and 2.0 MPa and the tensile strength of native human skin ranges between 5.0 and 30 MPa [13,44]. Interestingly, many studies have shown that decellularization decreases Young's modulus of leaf stiffness to that of most of the human tissues, which can be used as soft organs (1–20 kPa), muscles (10 kPa), and pre-calcified bone (100 kPa) [45].

### *3.2. Cellular Metabolic Activity and Cell Viability Assay*

Fibroblasts are stromal cells that constitute the majority of the stroma of tissue. It secretes various growth factors and cytokines by establishing epithelial–mesenchymal interactions, forming the ECM. They have a significant role in tissue development, maintenance, and repair. Incorporating cultured fibroblasts into various tissue-engineered constructs is used to treat burns and several other clinical applications [46,47]. The cellular metabolic activity of fibroblasts on DMS and DUJF scaffolds was evaluated for 1, 3, 5, and 7 days via a colorimetric MTT assay (Figure 5d). The colorimetric assay is dependent on mitochondrial respiration, where water-soluble tetrazolium dye is reduced to purple-colored formazan crystals via mitochondrial dehydrogenases. Both decellularized scaffolds (DMS and DUJF) show a significant difference in the cellular metabolic activity of fibroblasts compared with the TCP controls.

Moreover, DUJF scaffolds show more significant metabolic activity than DMS scaffolds throughout the culture period, which is presumed to be due to the pore size and porosity of DUJF providing fibroblast attachment, proliferation, and migration during the culture period compared to DMS. Furthermore, these nonfunctionalized decellularized scaffolds are non-cytotoxic and biocompatible for culturing mammalian cells. Nevertheless, the coating of decellularized scaffolds with ECM components such as motifs from collagen I, collagen IV, fibronectin, and laminin mimics the natural cellular environment and enhances cell attachment and proliferation in vitro [48]. Decellularized apple scaffolds coated with the collagen solution showed high Young's modulus with mineralization and osteogenic differentiation of pre-osteoblasts for bone tissue engineering [49].

The Live/Dead assay was used to quantitatively visualize the viability and proliferation of skin fibroblasts on decellularized scaffolds after 1, 3, 5, and 7 days of culture (Figure 6). Fibroblasts on scaffolds were stained with dual fluorescent dyes, viz., calcein-AM (live) and ethidium homodimer (dead) and observed under an inverted fluorescence microscope. DUJF scaffolds have significantly higher live and proliferating cells than DMS scaffolds; however, they are significantly less than the TCP control. The early difference in cell viability and cell proliferation on scaffolds and TCPs up to the 5th day can be mainly attributed to the presence of residual detergent and the disparity in the porosity, topography, and structural components of the framework of scaffolds [50]. However, after 7 days of culture, fibroblasts' proliferation and viability significantly increased in both scaffolds due to the secretion of ECM components of fibroblasts, which facilitate cell attachment, proliferation, and migration. Hence, both DMS and DUJF scaffolds were non-cytotoxic and biocompatible for fibroblast culturing and could be potential scaffolds for skin tissue engineering.

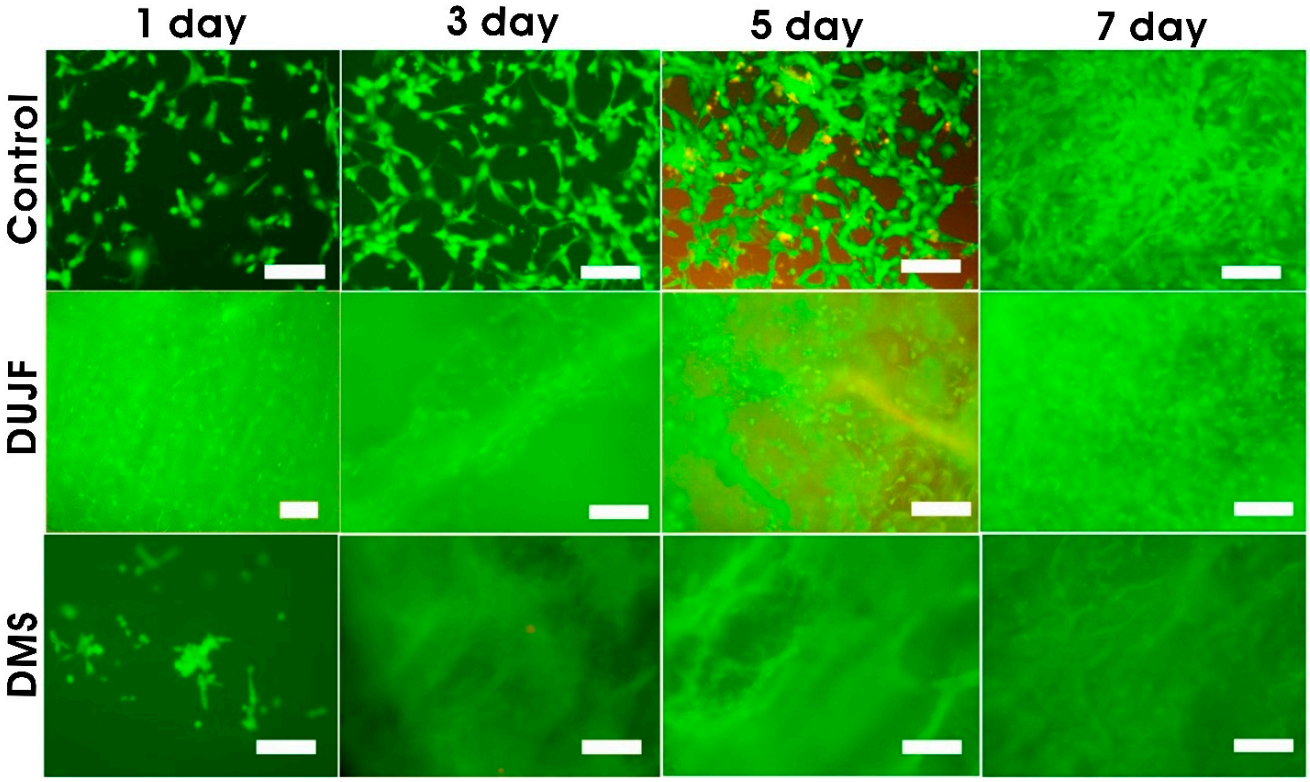


**Figure 6.** Qualitative analysis (Live/Dead assay) of decellularized DMS and DUJF scaffolds showing live (green) and dead (red) cells for 1, 3, 5, and 7 days of the culture period (scale bar = 50 μm).

The natural topographical architecture of plants and fungal scaffolds influences cell behaviors such as adhesion, proliferation, and migration, and the signaling between them regulates them at the molecular level. Figures 7 and 8 show the adherence and spreading of NIH/3T3 fibroblasts on the DUJF and DMS scaffolds on day 1, and proliferation continues throughout the incubation period. Migration of cells starts on day 3,and the formation of the ECM matrix was observed on day 5. The confluent cell layer was observed on day 7, which suggested the biocompatibility of DUJF and DMS scaffolds and the enhancement of cell migration through the interconnected pores with diffused nutrients for the maintenance of cell proliferation for tissue-engineered skin scaffolds. Compared to DUJF scaffolds, DMS scaffolds showed topographically increased proliferation of cells after day 7, which concurs with the metabolic activity of fibroblasts cultured on scaffolds. This could be correlated to the interconnected deep porous cavities, which allow the migration of more cells, the movement of nutrients, and the diffusion of gases. The diverse prefabricated vasculature of the decellularized vegetal kingdom reproduces structurally closer to the animal tissue and exhibits a wide range of mechanical properties to those of humans [51]. Cellulose-based vegetal materials as scaffolds support the attachment and survival of various cells, such as human endothelial cells [52], human dermal fibroblasts [53], myoblasts [29], and stem cells [54].

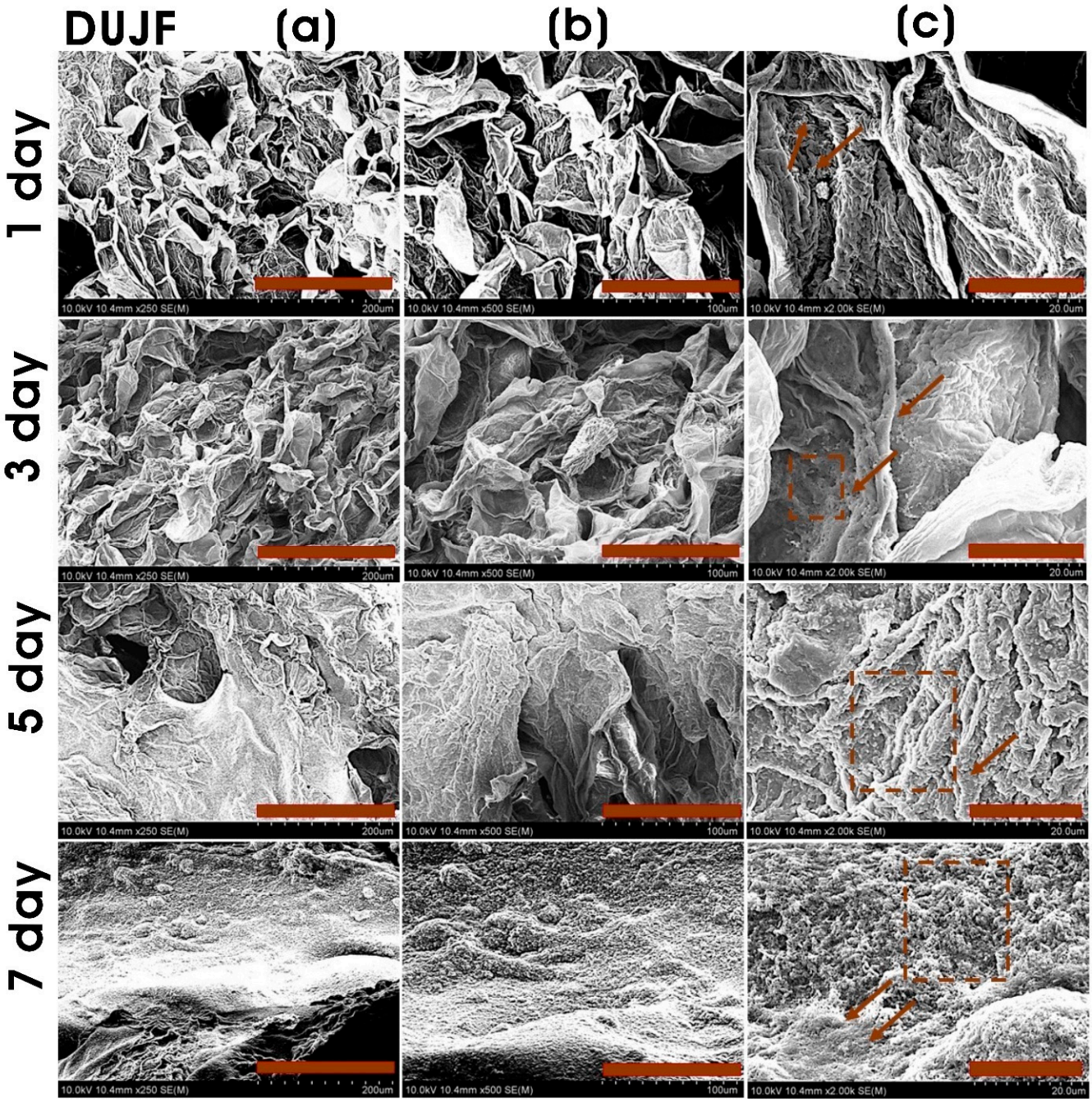


**Figure 7.** FE-SEM images of NIH/3T3 embryonic fibroblasts proliferation and migration on the DUJF scaffolds at different intervals. Scale bars: (**a**) 500 μm, (**b**) 100 μm, and (**c**) 20 μm. Square and arrow indicates cell morphology.

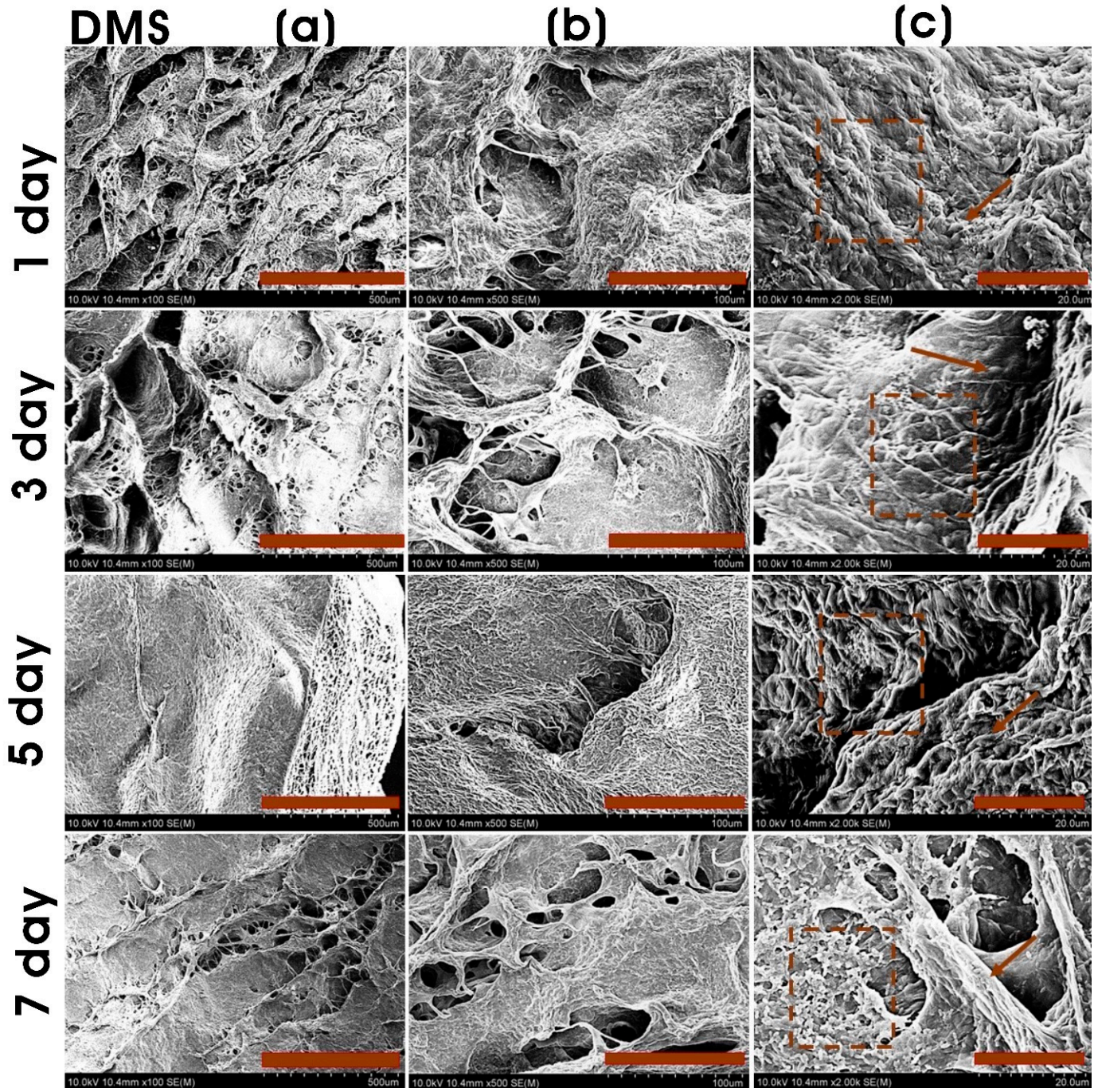


**Figure 8.** FE-SEM images of NIH/3T3 embryonic fibroblasts that proliferate and migrate on the DMS scaffolds at different intervals. Scale bars: (**a**) 500 µm, (**b**) 100 µm, and (**c**) 20 µm. Square and arrow indicates cell morphology.

## 4. Conclusions

To conclude, this study demonstrated that decellularized mushroom- and fruit-based scaffolds showed good morphological, physical, and mechanical properties for skin tissue engineering. Skin fibroblasts can attach to these decellularized scaffolds and proliferate even on the uncoated decellularized scaffolds. However, further modifications of the scaffold's surface with biocompatible and cell adhesion molecules can enhance the cell attachment, proliferation, and migration of cells and bring significant in vitro cytocompatibility to scaffolds. These decellularized natural scaffolds have functional groups, which can be used to enzymatically or chemically crosslink with desired moieties to improve

the scaffold's cell adhesion and mechanical properties for skin tissue engineering. Altogether, preparing decellularized cellulose-based and chitin/glucan-based scaffolds is inexpensive and eco-friendly. Further advancements in the fabrication of decellularized biomaterials with enhanced desired characteristics could be used as an ideal substitute for tissue-engineered skin substitutes for skin tissue engineering and wound healing. In the future, decellularized scaffolds can also be used as a good edible source for cultured meat production.

**Supplementary Materials:** The following supporting information can be downloaded at: https://www.mdpi.com/article/10.3390/su152115618/s1, Figure S1. Light microscopic images of (a) DUJF and (b) DMS (scale bar = 50 μm); Figure S2. DAPI staining of (a) native UJF (b) native MS, (c) DUJF and (d) DMS (scale bar = 50 μm); Figure S3. H&E staining of (a) native UJF (b) native MS, (c) DUJF and (d) DMS (scale bar = 50 μm).

**Author Contributions:** Conceptualization: K.B.N. and R.B.; Methodology and Data Collection: K.B.N. and R.B.; Funding Acquisition: S.S.H.; Writing—Original Draft Preparation: K.B.N., R.B. and H.K.; Writing—Review and Editing: K.B.N., R.B., H.K. and S.S.H. All authors have read and agreed to the published version of the manuscript.

**Funding:** This research was supported by the Korea Basic Science Institute (National Research Facilities and Equipment Center) grant funded by the Ministry of Education. This research was supported by the National Research Foundation of Korea (NRF) (Grant No. RS-2023-00278268, 2020R1A6A1A03044512 & No. 2019R1A6C1010046). This research was also funded by the Ministry of Agriculture, Food and Rural Affairs (MAFRA) (321027–5).

**Institutional Review Board Statement:** This article does not contain any studies involving human participants or experimental animals performed by any of the authors.

**Informed Consent Statement:** Not applicable.

**Data Availability Statement:** Data "available on request" by email.

**Acknowledgments:** Authors thank the Korea Institute of Planning and Evaluation for Technology in Food, Agriculture, and Forestry (IPET) through the High Value-added Food Technology Development Program, funded by the Ministry of Agriculture, Food and Rural Affairs (MAFRA) (321027–5). The characterization instruments were utilized at the Core Research Support Center for Natural Products and Medical Materials (CRCNM) at Yeungnam University.

**Conflicts of Interest:** The authors declare no conflict of interest.

## References

1. Uitto, J.; Olsen, D.R.; Fazio, M.J. Extracellular matrix of the skin: 50 years of progress. *J. Investig. Dermatol.* **1989**, *92*, S61–S77. [CrossRef]
2. Supp, D.M.; Boyce, S.T. Engineered skin substitutes: Practices and potentials. *Clin. Dermatol.* **2005**, *23*, 403–412. [CrossRef] [PubMed]
3. Singer, A.J.; Boyce, S.T. Burn wound healing and tissue engineering. *J. Burn Care Res.* **2017**, *38*, e605–e613. [CrossRef] [PubMed]
4. Fadilah, N.I.M.; Riha, S.M.; Mazlan, Z.; Wen, A.P.Y.; Hao, L.Q.; Joseph, B.; Maarof, M.; Thomas, S.; Motta, A.; Fauzi, M.B. Functionalised-Biomatrix for Wound Healing and Cutaneous Regeneration: Future Impactful Medical Products in Clinical Translation and Precision Medicine. *Front. Bioeng. Biotechnol.* **2023**, *11*, 734. [CrossRef]
5. Vig, K.; Chaudhari, A.; Tripathi, S.; Dixit, S.; Sahu, R.; Pillai, S.; Dennis, V.A.; Singh, S.R. Advances in skin regeneration using tissue engineering. *Int. J. Mol. Sci.* **2017**, *18*, 789. [CrossRef]
6. Tibbitt, M.W.; Anseth, K.S. Hydrogels as extracellular matrix mimics for 3D cell culture. *Biotechnol. Bioeng.* **2009**, *103*, 655–663. [CrossRef] [PubMed]
7. Calore, A.R.; Srinivas, V.; Groenendijk, L.; Serafim, A.; Stancu, I.C.; Wilbers, A.; Leoné, N.; Sanchez, A.A.; Auhl, D.; Mota, C. Manufacturing of scaffolds with interconnected internal open porosity and surface roughness. *Acta Biomater.* **2023**, *156*, 158–176. [CrossRef] [PubMed]
8. Akilbekova, D.; Shaimerdenova, M.; Adilov, S.; Berillo, D. Biocompatible scaffolds based on natural polymers for regenerative medicine. *Int. J. Biol. Macromol.* **2018**, *114*, 324–333. [CrossRef]
9. Kim, Y.S.; Majid, M.; Melchiorri, A.J.; Mikos, A.G. Applications of decellularized extracellular matrix in bone and cartilage tissue engineering. *Bioeng. Transl. Med.* **2019**, *4*, 83–95. [CrossRef]

10. Gilpin, A.; Yang, Y. Decellularization strategies for regenerative medicine: From processing techniques to applications. *BioMed Res. Int.* **2017**, *2017*, 9831534. [CrossRef]
11. Liguori, G.R.; Jeronimus, B.F.; de Aquinas Liguori, T.T.; Moreira, L.F.P.; Harmsen, M.C. Ethical issues in the use of animal models for tissue engineering: Reflections on legal aspects, moral theory, three rs strategies, and harm–benefit analysis. *Tissue Eng. Part C Methods* **2017**, *23*, 850–862. [CrossRef] [PubMed]
12. Chan, E.C.; Kuo, S.-M.; Kong, A.M.; Morrison, W.A.; Dusting, G.J.; Mitchell, G.M.; Lim, S.Y.; Liu, G.-S. Three dimensional collagen scaffold promotes intrinsic vascularisation for tissue engineering applications. *PLoS ONE* **2016**, *11*, e0149799. [CrossRef]
13. Narayanan, K.B.; Zo, S.M.; Han, S.S. Novel biomimetic chitin-glucan polysaccharide nano/microfibrous fungal-scaffolds for tissue engineering applications. *Int. J. Biol. Macromol.* **2020**, *149*, 724–731. [CrossRef] [PubMed]
14. Hickey, R.J.; Modulevsky, D.J.; Cuerrier, C.M.; Pelling, A.E. Customizing the shape and microenvironment biochemistry of biocompatible macroscopic plant-derived cellulose scaffolds. *ACS Biomater. Sci. Eng.* **2018**, *4*, 3726–3736. [CrossRef] [PubMed]
15. Sambrook, J.; Russell, D.W. Purification of nucleic acids by extraction with phenol: Chloroform. *Cold Spring Harb. Protoc.* **2006**, *2006*, pdb. prot4455. [CrossRef]
16. García-Alegría, A.M.; Anduro-Corona, I.; Pérez-Martínez, C.J.; Guadalupe Corella-Madueño, M.A.; Rascón-Durán, M.L.; Astiazaran-Garcia, H. Quantification of DNA through the NanoDrop spectrophotometer: Methodological validation using standard reference material and Sprague Dawley rat and human DNA. *Int. J. Anal. Chem.* **2020**, *2020*, 8896738. [CrossRef]
17. Sargazi, Z.; Zavareh, S.; Jafarabadi, M.; Salehnia, M. An efficient protocol for decellularization of the human endometrial fragments for clinical usage. *Prog. Biomater.* **2021**, *10*, 119–130. [CrossRef]
18. Tan, Y.; Landford, W.N.; Garza, M.; Suarez, A.; Zhou, Z.; Coon, D. Complete human penile scaffold for composite tissue engineering: Organ decellularization and characterization. *Sci. Rep.* **2019**, *9*, 16368. [CrossRef]
19. Podgórski, R.; Wojasiński, M.; Ciach, T. Nanofibrous materials affect the reaction of cytotoxicity assays. *Sci. Rep.* **2022**, *12*, 9047. [CrossRef]
20. Toker-Bayraktar, M.; Erenay, B.; Altun, B.; Odabaş, S.; Garipcan, B. Plant-derived biomaterials and scaffolds. *Cellulose* **2023**, *30*, 2731–2751. [CrossRef]
21. Predeina, A.L.; Dukhinova, M.S.; Vinogradov, V.V. Bioreactivity of decellularized animal, plant, and fungal scaffolds: Perspectives for medical applications. *J. Mater. Chem. B* **2020**, *8*, 10010–10022. [PubMed]
22. Feng, J.; Xiu, Q.; Huang, Y.; Troyer, Z.; Li, B.; Zheng, L. Plant-Derived Vesicle-Like Nanoparticles as Promising Biotherapeutic Tools: Present and Future. *Adv. Mater.* **2023**, *35*, 2207826.
23. Nasrabadi, M.N.; Doost, A.S.; Mezzenga, R. Modification approaches of plant-based proteins to improve their techno-functionality and use in food products. *Food Hydrocoll.* **2021**, *118*, 106789.
24. Esmaeili, J.; Jadbabaee, S.; Far, F.M.; Lukolayeh, M.E.; Kırboğa, K.K.; Rezaei, F.S.; Barati, A. Decellularized alstroemeria flower stem modified with chitosan for tissue engineering purposes: A cellulose/chitosan scaffold. *Int. J. Biol. Macromol.* **2022**, *204*, 321–332. [PubMed]
25. Ahmadian, M.; Hosseini, S.; Alipour, A.; Jahanfar, M.; Farrokhi, N.; Homaeigohar, S.; Shahsavarani, H. In vitro modeling of hepatocellular carcinoma niche on decellularized tomato thorny leaves: A novel natural three-dimensional (3D) scaffold for liver cancer therapeutics. *Front. Bioeng. Biotechnol.* **2023**, *11*, 1189726. [CrossRef] [PubMed]
26. Novaes-Ledieu, M.; Mendoza, C.G. The cell walls of Agaricus bisporus and Agaricus campestris fruiting body hyphae. *Can. J. Microbiol.* **1981**, *27*, 779–787. [CrossRef] [PubMed]
27. Michalenko, G.; Hohl, H.; Rast, D. Chemistry and architecture of the mycelial wall of Agaricus bisporus. *Microbiology* **1976**, *92*, 251–262. [CrossRef]
28. Noda, T.; Hatakeyama, M.; Kitaoka, T. Combination of Polysaccharide Nanofibers Derived from Cellulose and Chitin Promotes the Adhesion, Migration and Proliferation of Mouse Fibroblast Cells. *Nanomaterials* **2022**, *12*, 402. [CrossRef]
29. Cheng, Y.-W.; Shiwarski, D.J.; Ball, R.L.; Whitehead, K.A.; Feinberg, A.W. Engineering aligned skeletal muscle tissue using decellularized plant-derived scaffolds. *ACS Biomater. Sci. Eng.* **2020**, *6*, 3046–3054. [CrossRef]
30. Salehi, A.; Mobarhan, M.A.; Mohammadi, J.; Shahsavarani, H.; Shokrgozar, M.A.; Alipour, A. Efficient mineralization and osteogenic gene overexpression of mesenchymal stem cells on decellularized spinach leaf scaffold. *Gene* **2020**, *757*, 144852. [CrossRef]
31. Nesic, D.; Whiteside, R.; Brittberg, M.; Wendt, D.; Martin, I.; Mainil-Varlet, P. Cartilage tissue engineering for degenerative joint disease. *Adv. Drug Deliv. Rev.* **2006**, *58*, 300–322. [CrossRef] [PubMed]
32. Modulevsky, D.J.; Lefebvre, C.; Haase, K.; Al-Rekabi, Z.; Pelling, A.E. Apple derived cellulose scaffolds for 3D mammalian cell culture. *PLoS ONE* **2014**, *9*, e97835.
33. Modulevsky, D.J.; Cuerrier, C.M.; Pelling, A.E. Biocompatibility of subcutaneously implanted plant-derived cellulose biomaterials. *PLoS ONE* **2016**, *11*, e0157894.
34. Paleologos, E.K.; Giokas, D.L.; Karayannis, M.I. Micelle-mediated separation and cloud-point extraction. *TrAC Trends Anal. Chem.* **2005**, *24*, 426–436.
35. Abderrahim, B.; Abderrahman, E.; Mohamed, A.; Fatima, T.; Abdesselam, T.; Krim, O. Kinetic thermal degradation of cellulose, polybutylene succinate and a green composite: Comparative study. *World J. Environ. Eng.* **2015**, *3*, 95–110.
36. Movasaghi, Z.; Rehman, S.; ur Rehman, D.I. Fourier transform infrared (FTIR) spectroscopy of biological tissues. *Appl. Spectrosc. Rev.* **2008**, *43*, 134–179. [CrossRef]

37. Oliveira, R.N.; Mancini, M.C.; Oliveira, F.C.S.D.; Passos, T.M.; Quilty, B.; Thiré, R.M.D.S.M.; McGuinness, G.B. FTIR analysis and quantification of phenols and flavonoids of five commercially available plants extracts used in wound healing. *Matéria* **2016**, *21*, 767–779.
38. Bekiaris, G.; Tagkouli, D.; Koutrotsios, G.; Kalogeropoulos, N.; Zervakis, G.I. Pleurotus mushrooms content in glucans and ergosterol assessed by ATR-FTIR spectroscopy and multivariate analysis. *Foods* **2020**, *9*, 535. [CrossRef]
39. Crapo, P.M.; Gilbert, T.W.; Badylak, S.F. An overview of tissue and whole organ decellularization processes. *Biomaterials* **2011**, *32*, 3233–3243.
40. Kamata, H.; Akagi, Y.; Kayasuga-Kariya, Y.; Chung, U.-I.; Sakai, T. "Nonswellable" hydrogel without mechanical hysteresis. *Science* **2014**, *343*, 873–875. [CrossRef]
41. Zhao, C.; Lin, Z.; Yin, H.; Ma, Y.; Xu, F.; Yang, W. PEG molecular net-cloth grafted on polymeric substrates and its bio-merits. *Sci. Rep.* **2014**, *4*, 4982. [CrossRef] [PubMed]
42. Geikowsky, E.; Gorumlu, S.; Aksak, B. The effect of flexible joint-like elements on the adhesive performance of nature-inspired bent mushroom-like fibers. *Beilstein J. Nanotechnol.* **2018**, *9*, 2893–2905. [CrossRef] [PubMed]
43. Contessi Negrini, N.; Toffoletto, N.; Farè, S.; Altomare, L. Plant tissues as 3D natural scaffolds for adipose, bone and tendon tissue regeneration. *Front. Bioeng. Biotechnol.* **2020**, *8*, 723. [CrossRef] [PubMed]
44. Mow, V.C.; Guo, X.E. Mechano-electrochemical properties of articular cartilage: Their inhomogeneities and anisotropies. *Annu. Rev. Biomed. Eng.* **2002**, *4*, 175–209. [CrossRef] [PubMed]
45. Harris, A.F.; Lacombe, J.; Zenhausern, F. The emerging role of decellularized plant-based scaffolds as a new biomaterial. *Int. J. Mol. Sci.* **2021**, *22*, 12347. [CrossRef]
46. Soundararajan, M.; Kannan, S. Fibroblasts and mesenchymal stem cells: Two sides of the same coin? *J. Cell. Physiol.* **2018**, *233*, 9099–9109. [CrossRef]
47. Wong, T.; McGrath, J.; Navsaria, H. The role of fibroblasts in tissue engineering and regeneration. *Br. J. Dermatol.* **2007**, *156*, 1149–1155. [CrossRef]
48. Cooke, M.; Phillips, S.; Shah, D.; Athey, D.; Lakey, J.; Przyborski, S. Enhanced cell attachment using a novel cell culture surface presenting functional domains from extracellular matrix proteins. *Cytotechnology* **2008**, *56*, 71–79. [CrossRef]
49. Latour, M.L.; Tarar, M.; Hickey, R.J.; Cuerrier, C.M.; Catelas, I.; Pelling, A.E. Plant-derived cellulose scaffolds for bone tissue engineering. *BiorXiv* **2020**. [CrossRef]
50. Partearroyo, M.A.; Ostolaza, H.; Goñi, F.M.; Barberá-Guillem, E. Surfactant-induced cell toxicity and cell lysis: A study using B16 melanoma cells. *Biochem. Pharmacol.* **1990**, *40*, 1323–1328. [CrossRef]
51. McCulloh, K.A.; Sperry, J.S.; Adler, F.R. Water transport in plants obeys Murray's law. *Nature* **2003**, *421*, 939–942. [CrossRef] [PubMed]
52. Gershlak, J.R.; Hernandez, S.; Fontana, G.; Perreault, L.R.; Hansen, K.J.; Larson, S.A.; Binder, B.Y.; Dolivo, D.M.; Yang, T.; Dominko, T. Crossing kingdoms: Using decellularized plants as perfusable tissue engineering scaffolds. *Biomaterials* **2017**, *125*, 13–22. [CrossRef] [PubMed]
53. Fontana, G.; Gershlak, J.; Adamski, M.; Lee, J.S.; Matsumoto, S.; Le, H.D.; Binder, B.; Wirth, J.; Gaudette, G.; Murphy, W.L. Biofunctionalized plants as diverse biomaterials for human cell culture. *Adv. Healthc. Mater.* **2017**, *6*, 1601225. [CrossRef] [PubMed]
54. Phan, N.V.; Wright, T.; Rahman, M.M.; Xu, J.; Coburn, J.M. In vitro biocompatibility of decellularized cultured plant cell-derived matrices. *ACS Biomater. Sci. Eng.* **2020**, *6*, 822–832. [CrossRef]